Research Article

Applying UPC Scaling-Up Methodology to the LSTF-PKL Counterpart Test

V. Martinez-Quiroga, F. Reventos, and J. Freixa

Technical University of Catalonia, Institute of Energy Technologies, Avenida Diagonal 647, 08028 Barcelona, Spain

Correspondence should be addressed to V. Martinez-Quiroga; victor.martinez@nortuen.com

In the framework of the nodalization qualification process and quality guarantee procedures and following the guidelines of Kv-scaled analysis and UMAE methodology, further development has been performed by UPC team resulting in a scaling-up methodology. Such methodology has been applied in this paper for analyzing discrepancies that appear between the simulations of two counterpart tests. It allows the analysis of scaling-down criterion used for the design of an ITF and also the investigation of the differences of configuration between an ITF and a particular NPP. For analyzing both, it applies two concepts "scaled-up nodalizations" and "hybrid nodalizations." The result of this activity is the explanation of appeared distortions and its final goal is to qualify nodalizations for their use in the analysis of equivalent scenarios at an NPP scale. In this sense, the experimental data obtained in the OECD/NEA PKL-2 and ROSA-2 projects as counterpart test are of a great value for the testing of the present methodology. The results of the posttest calculations of LSTF-PKL counterpart tests have allowed the analyst to define which phenomena could be well reproduced by their nodalizations and which not, in this way establishing the basis for a future extrapolation to an NPP scaled calculation. The application of the UPC scaling up methodology has demonstrated that selected phenomena can be scaled-up and explained between counterpart simulations by carefully considering the differences in scale and design.

1. Introduction

Computational analyses of full-scale nuclear power plants (NPP) have a wide and consolidated application on nuclear engineering. Most of the uses of NPP nodalizations, related to the support to plant operation and control, have been extensively described in two different safety reports [1, 2] by the International Atomic Energy Agency (IAEA) [1, 2]. The first one [1] is specifically devoted to detail the guidelines for the development of power plant nodalizations by the use of system codes. During the last 20 years, the Technical University of Catalonia (UPC) has completed several works in this field following similar strategies as in [1]. The description of some of these contributions can be found in [3–7] which deal with the development and usage of NPP nodalizations in the support to plant operation and control. This experience has shown the usefulness and possibilities of this approach. One of the major outcomes is that the continuous development

and improvement of NPP nodalizations are not only a requirement but also a difficult task due to the large amount of information contained in a full NPP nodalization. In that sense, methodologies designed to qualify NPP nodalizations take a key role and can be used to both provide an insight in the quality of the produced analyses and, in addition, help the developer in the detection of possible deficiencies in the nodalization.

In a related paper [8], the UPC scaling-up methodology was presented as a tool to contribute to qualifying NPP nodalizations. The UPC scaling-up methodology is a systematic procedure for qualifying NPP nodalizations taking advantage of the experience acquired through the posttest analysis of integral test facility (ITF) experiments. It is devoted to the nodalization qualification, which implies that the methodology can only be applied to those phenomena that have been well reproduced on ITF posttest analyses; and that the scaling analyses are only performed through code simulations.
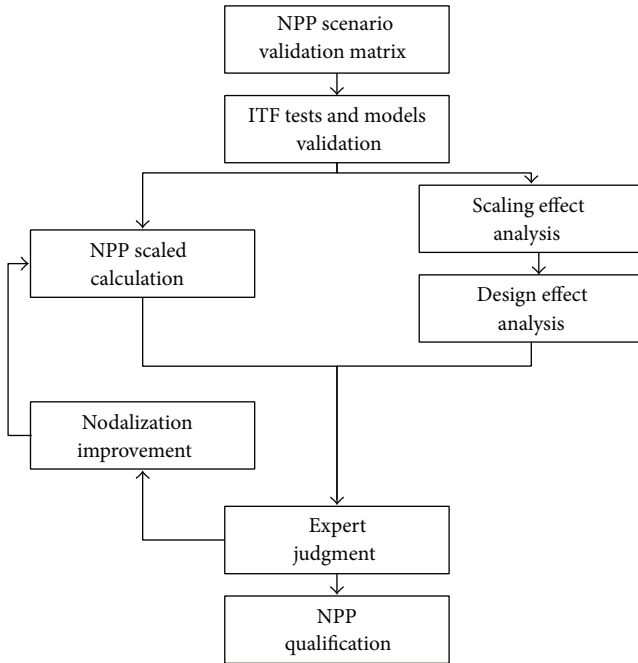
Figure 1: UPC scaling-up methodology.

The two main factors that affect the scaling-up of the ITF posttest simulations are the scaling-down criterion used for the design of the ITF and the differences of configuration between the ITF and the NPP. For analyzing both, the UPC scaling-up methodology applies two concepts, "scaled-up nodalizations" and "Hybrid nodalizations." The so called "scaled-up nodalizations" can be used to analyze the effect of the ITF scaling criterion in a scaled-up calculation. On the other hand, the "hybrid nodalizations" are defined as modified scaled-up ITF nodalizations in which some components have been adjusted to resemble the configuration of the NPP system. The aim of these nodalizations is to evaluate the influence of each aspect of the configuration on the ITF simulation results independently of the scale. A diagram associated with the "UPC scaling-up methodology" is shown in Figure 1, and further details on each step can be found in [8].

In the present work, the UPC scaling-up methodology is applied in order to check its capabilities for justifying and detecting the discrepancies that may appear between counterpart simulations performed with different nodalizations at different scales. For this purpose, the experiments performed within the framework of the OECD/NEA ROSA-2 and PKL-2 projects are used. These two projects are related to experiments at the two correspondent ITFs: the Primärkreislauf (PKL) test facility [9] operated by AREVA and the Large-Scale Test Facility (LSTF) [10] operated by the Japan Atomic Energy Agency (JAEA). During 2011, a link was established between the two projects in order to perform a counterpart experiment with the two facilities. The objective of the counterpart test was to represent the same accident conditions with two different scaling criteria and at different local geometries in order to evaluate their effect on the evolution of the transient. In this work, the ROSA-2 Test

3 and the PKL-2 Test G7.1 (also known as counterpart tests) will be simulated, qualified, and analyzed applying design effect analyses and scale effect analyses which are part of this particular methodology (see Figure 1).

2. Facilities and Test Description

2.1. LSTF. LSTF is an experimental facility operated by JAEA; it is designed to simulate a Westinghouse-type 4-loop 3,420 MWth PWR under emergency conditions. It is a full-height and 1/48 volumetrically-scaled two-loop system with a maximum core power of 10 MW (14% of the scaled PWR nominal core power) and pressures scaled 1 : 1. Loops are sized to conserve volumetric factor (2/48) and to simulate the same flow regime transitions in the horizontal legs (preserving $L/\sqrt{D}$ factor).

There is one SG for each loop respecting the same scaling factors. They have 141 full-size U-tubes, inlet and outlet plena, steam separator, steam dome, steam dryer, main steam line, four downcomers, and other internals.

All emergency systems are represented and have a big versatility referred to their functions and positions. Many break locations (a total of 20) are available too.

LSTF test facility has about 1,760 measurement points that allow an exhaustive analysis of the tests. There are two types of data or measurements of interest: directly measured quantities (temperature, pressure, and differential pressure) and derived quantities (from the combination of two or more direct measured quantities: coolant density, mass flow rate etc.).

2.2. PKL. PKL is an ITF which reproduces the entire primary system and most of the secondary system (except for the turbine and condenser) of a 1300 MW PWR plant operated by AREVA. It is based on a four-loop Siemens design (KWU), with elevations scaled 1 : 1 and volumes and power reduced by a factor of 145. The number of rods in the core and the U-tubes in the steam generator has been divided by 145 as well following the power-to-volume scaling criterion. The core has been modeled by 314 electrical heater rods. Unlike many experimental facilities with only two available loops (one for the broken loop and one to simulate the other three intact loops) PKL simulates all four loops separately. This is very important in order to analyze asymmetrical transients, for example, with injection in two out of four loops.

The operating pressure of the PKL facility is limited to 45 bars on the primary side and to 56 bars on the secondary side. This allows simulation over a wide temperature range (522 K to 322 K) that is particularly applicable to the cooldown procedures investigated, although it limits the simulation of the high-pressure phases of some events, for instance, the initial phase of an SBLOCA.

All emergency systems are represented and have a wide versatility referred to their functions and positions. The pump injection system is available in all the hot and cold legs. Many break locations are available too.

PKL test facility has about 1500 measurement points that permit an exhaustive analysis of the tests. Sixty of

TABLE 1: PKL and LSTF major features.

	LSTF	PKL
Reference plant	Westinghouse	KWU (Siemens design)
Height	Full	Full
Volumetric scaling	1/48	1/145
Number of loops	2	4
Pressure vessel DC	Cylindrical	Double-pipe
U-tubes/SG	141	30
Pressure	Full	Up to 4.5 MPa
Core power	14% (10 MW)	10% (2.5 MW)
Number of electrical rods	1008	314
Axial profile	Chopped cosine	Flat
Radial profile	3-region	3-region
ECCS	Full	Full
Hot leg diameter (m)	0.207	0.128
Special measurement	Video probe, O_2 gas sensor	Boron sensor
Number of instruments	About 1760	About 1070

the measurement devices are identical to those that are used in a commercial plant to simulate what an operator would control in case of an accident.

Major features of both power-to-volume scaled-down facilities are detailed in Table 1.

2.3. PKL-2 and LSTF-2 Counterpart Test. In 2011, a counterpart test was performed in LSTF and PKL test facilities as a part of the OECD/NEA ROSA-2 and PKL-2 projects (test 3 and test G7.1, resp.). The objective of both tests was devoted to analyze two aspects:

(i) core exit temperature (CET) measurement effectiveness in accident management (AM) of NPPs;

(ii) scaling effects between PKL and LSTF test facilities.

The selected scenario was an upward oriented 1.5% hot leg SBLOCA. System failures as no high-pressure safety injection and no automatic secondary-side safety cooldown were imposed. The particular test conditions are described in the sections below.

2.3.1. ROSA-2 Test 3 Test Conditions. This test was divided into three phases, a high-pressure phase, reproducing the NPP scenario at full pressure; a low-pressure phase, reproducing the same scenario at counterpart conditions with PKL; and finally, an intermediate phase, with the purpose of conditioning the LSTF conditions at the end of the high-pressure phase to the PKL counterpart test conditions. Table 2 shows the list of imposed conditions for each phase.

Several parameters were adjusted from the PKL test conditions with the aim of having analogous behaviors during the low-pressure phase of the transient. A scaling factor $K_v = 2.55$ was applied for calculating the opening area of

the SG's relief valves, the water volumes of the accumulators, and the injection rates of the low-pressure injection (LPI) system. Pressures in the primary and secondary systems were adjusted 1 : 1 to the PKL test conditions during the conditioning phase, and the mass inventory was reinstated in order to have a similar hot leg liquid level as expected to occur in the PKL test. Reflux and condenser conditions were established in both facilities at the beginning of the counterpart phase. Accumulators' set point was reduced to 2.6 MPa for including their actuation in both facilities.

2.3.2. PKL-2 G7.1 Test Conditions. The PKL initial conditions were adjusted at its maximum pressures in order to reproduce as realistic as it can PWR SBLOCA reflux and condensation, core dryout, and accident management phases. The test conditions were set identical as those of LSTF low-pressure phase conditions (see Table 2).

In relation to scaling, the mass inventory in the secondary side was adjusted using K_v factor in order to have the same ratio between liquid and energy storage in the SG's. The Core power was slightly increased above the K_v factor to compensate the differences present between both facilities in the external heat losses.

2.3.3. Experimental Results. The results of the counterpart phases showed a close agreement for reproducing the main phenomena expected for the transient. Both facilities reproduced similarly the three parts of the transient (reflux and condensation, vapor superheating, and accident management; see Figures 2 and 3) obtaining a wide spectrum of experimental data for analyzing the relationship between CET and PCT and the effectiveness of the CET signal for AM actuations.

Some differences were detected between the results of both facilities.

(i) Core dryout: there is a delay of 280 s in the core dryout (see Figure 4) which modifies the timing of next phases of the transients.

(ii) CET versus PCT curve: the relationship between the CET and the PCT measurements shows different slope when the CET starts to increase (see Figure 5). Because of that, there is a discrepancy of 55 K in the PCT of both facilities when the condition of the AM action is achieved ($T_{CET} > 623$ K).

(iii) Effectiveness of the SG depressurization takes place at a different rate in each facility. Figure 6 compares PCTs of both tests for the interval in which SG depressurization and accumulators' injection take place. Results show that for PKL facility rewetting cannot be assured without the entrance of the passive ECCS system.

TABLE 2: Test 3 test conditions.

Event	Condition	High-pressure phase	Conditioning phase	Low-pressure phase
Break valve opened	$t = 0$ s	*		
Low-pressure scram signal	$P_{prim} < 12.96$ MPa	*		
Secondary system isolation	Scram signal	*		
Initiation of primary coolant pump coastdown	Scram signal	*		
Initiation of core power decay curve simulation	Scram signal	*		
Initiation of HPI coolant injection into pressure vessel upper plenum	$T_{PCT} > 750$ K	*		
Break valve closed	$P_{prim} < 5$ MPa	*	*	
Power constant	$P_{prim} < 5$ MPa		*	
Termination of HPI coolant injection into pressure vessel upper plenum	$H_{HL} \cong \frac{1}{2} \cdot H$		*	
SG's relief valve depressurization	$H_{HL} \cong \frac{1}{2} \cdot H_{HL}$		*	
Secondary system isolation	$P_{prim} < 3.9$ MPa		*	
Break valve reopened	$P_{prim} > 4.5$ MPa		*	*
SG depressurization as AM action	$T_{CET} > 623$ K			*
Initiation of AFW in both loops	AM action signal			*
Initiation of ACC system in both loops	$P_{prim} < 2.6$ MPa			*
Termination of ACC system in both loops	$P_{prim} < 1.2$ MPa			*
Initiation of LPI system in both loops	$P_{prim} < 1$ MPa			*
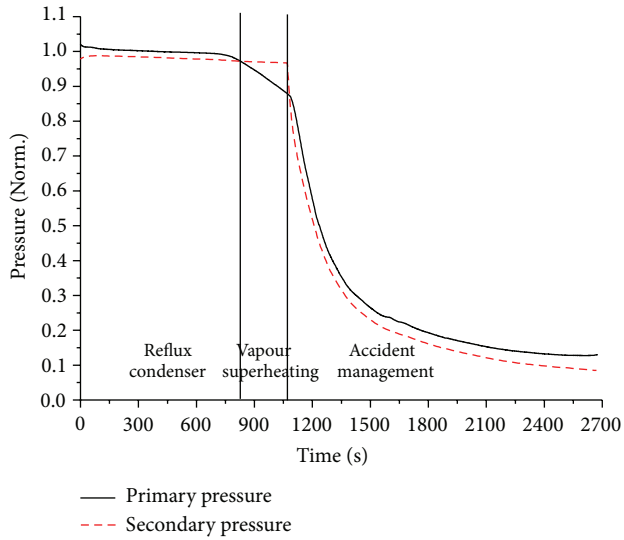
FIGURE 2: LSTF system pressures.
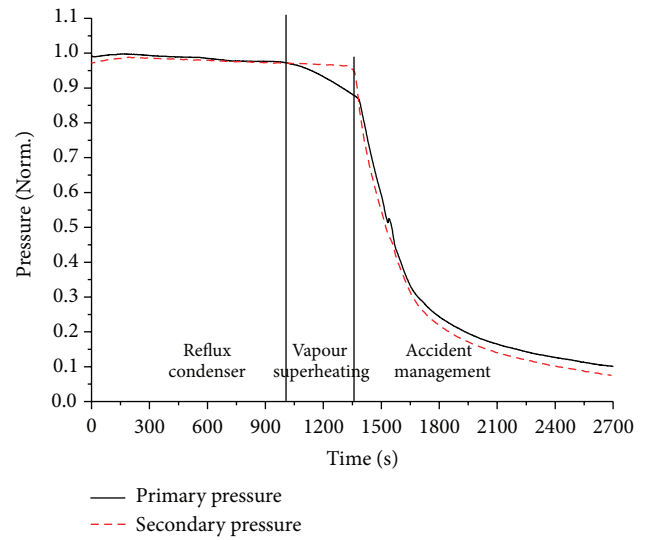
FIGURE 3: PKL system pressures.

3. Results

3.1. PKL G7.1 Posttest Analysis. Two calculations were performed by making use of the qualified (see [11–14]) UPC PKL RELAP5mod3.3 nodalization:

 (i) UPC PKL 1D nodalization;

 (ii) UPC PKL pseudo-3D nodalization.

The differences between both nodalizations were exclusively related to the core and upper plenum modeling. UPC PKL 1D nodalization simulated them with one channel (in addition to the core bypass), having fuel and all passive heat structures (core barrel and unheated rods) linked to the same volumes. The fuel was modeled with three HSs, with the same power ratio, and divided into 7 axial levels.
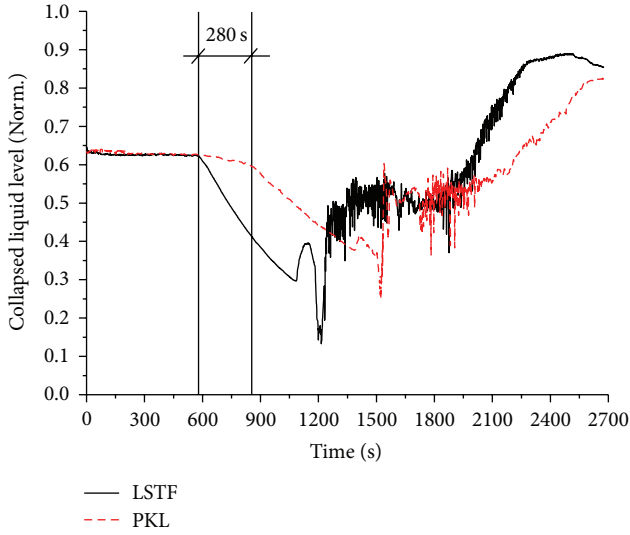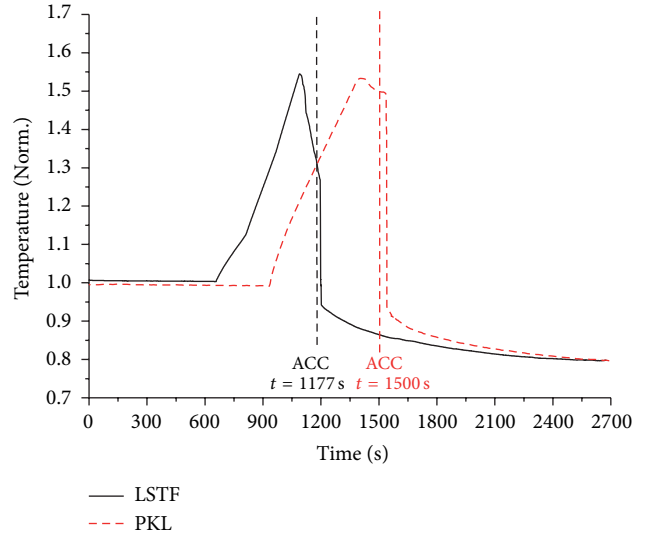
FIGURE 4: Core level.
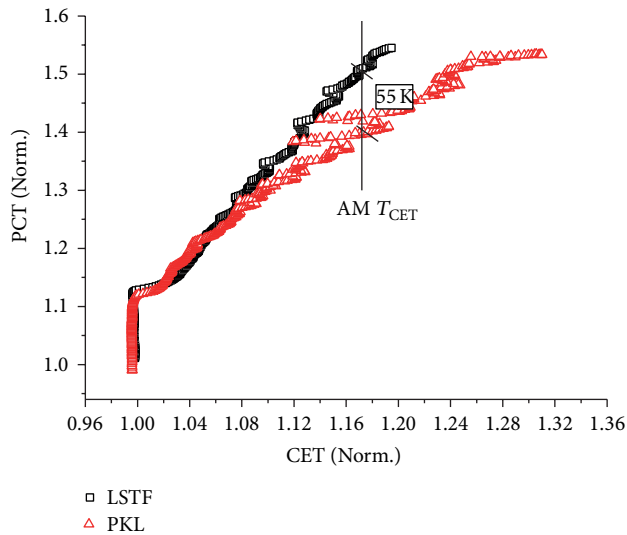

FIGURE 6: Peak cladding temperature.
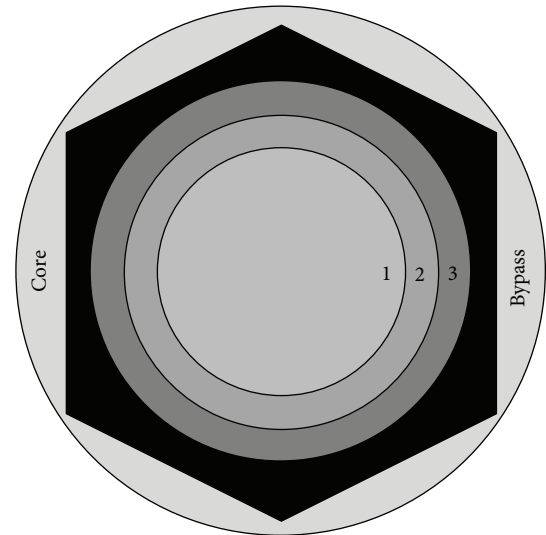

FIGURE 5: CET versus PCT curve.

FIGURE 7: UPC PKL pseudo-3D nodalization core channels.

UPC PKL pseudo-3D nodalization had the core and upper plenum (until the CET thermocouple level) divided into three radial channels (see Figure 7), with one fuel HS for each channel. The HSs for the passive internal metal structures were split for each channel proportionally to the flow path of each one, and the core barrel was linked to the outer zone. The radial flow paths between cells were modeled and transversal momentum equations were activated following the recommendations of reference [15]. The total number of core axial meshes was increased to 14 and the upper plenum cell heights were adjusted so that the center of the node coincided with the elevation of the thermocouples in the test facility.

The obtained results showed a quite close agreement for both nodalizations reproducing the initial conditions (see Table 3) as well as the general behavior of the transient (Figures 8 and 9 show a close agreement of both nodalizations for reproducing depressurization rate during three reported phases of the transient: reflux and condensation, vapor superheating, and SG depressurization). The pseudo-3D nodalization provided closer results for the main events because it reduced the delay in the core uncovery (see Table 4). This was seen to be a consequence because of a higher vapor generation in the 1D nodalization during the phases of reflux and condensation and vapor superheating. It implied that, for similar break mass losses, liquid mass inventory decreased faster and core uncovery started before. In Figure 10, the differences between vapor generation and break mass flows are compared (the differences are calculated by subtracting the values of the pseudo-3D nodalization to the 1D nodalization).

TABLE 3: Initial conditions of PKL G7.1 Test.

	Experimental data	UPC 1D nodalization	UPC pseudo-3D nodalization
Core power (Norm.)	1	0.996	0.996
Pressurizer pressure (Norm.)	1	1	1
Pressurizer liquid level (Norm.)	1	0.7	0.7
Secondary-side pressure (Norm.)	1	1	0.998
Secondary-side liquid level (Norm.)	1	0.998	1
Main feedwater temperature (Norm.)	1	1	1
Accumulators pressure (Norm.)	1	1	1
Accumulators temperature (Norm.)	1	1	1
LPI pressure (initiation of system) (Norm.)	1	1	1
LPI temperature (Norm.)	1	1	1
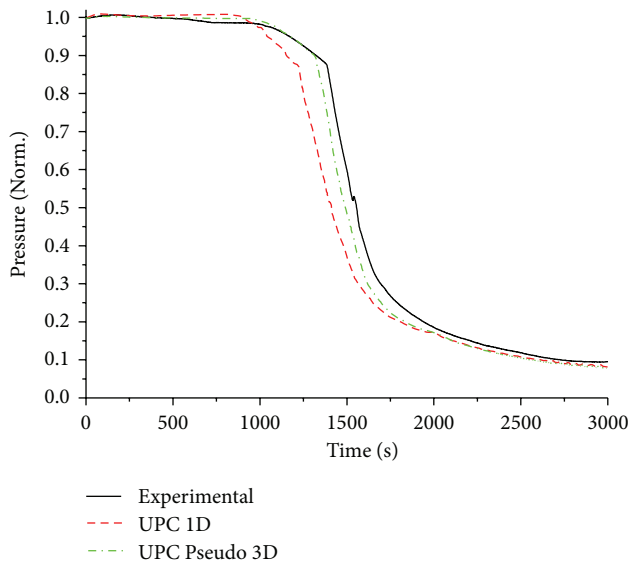
FIGURE 8: Primary pressure.

FIGURE 10: Mass flow comparison.

FIGURE 9: Secondary pressure.

Finally, the UPC PKL pseudo-3D nodalization was qualified for reproducing the relationship between the CET and the PCT. This nodalization solved instabilities in the simulation of the overheated CET (Figure 11), obtaining close results in the CET versus PCT curve (Figure 12). The pseudo-3D nodalization reproduced the same slope of the experimental data as well as the initial increase of the PCT.

On the other hand, the pseudo-3D nodalization was not qualified for reproducing closely the core quenching after SG depressurization action. Despite, the fact that core refilling was simulated, in the calculation quench front achieved the top level of the active core before accumulators' injection, showing a discrepancy in experimental results. In Figure 11, each CET curve is associated with a vertical line that indicates the time at which the accumulators' injection starts. The comparison shows that for both simulations, the temperatures dropped before accumulators' injection, unlike experimental data, in which it did not occur.

3.2. LSTF Test 3 Posttest Analysis. A base case calculation was performed using the UPC LSTF RELAP5mod3.3 nodalization that had been qualified previously for the ROSA Test

TABLE 4: Main events of PKL G7.1 Test.

	Experimental (s)	UPC 1D nodalization (s)	UPC pseudo-3D nodalization (s)
Start of the transient	0	0	0
Beginning of core uncovery	940	800	940
Primary pressure below secondary pressure	1020	920	1010
Secondary-side depressurization	1360	1190	1295
Start of accum. injection	1500	1304	1450
ACC injection finished	1860	1712	1752
LPSI started	2060	1966	1993
End of the test	5685	5685	5685
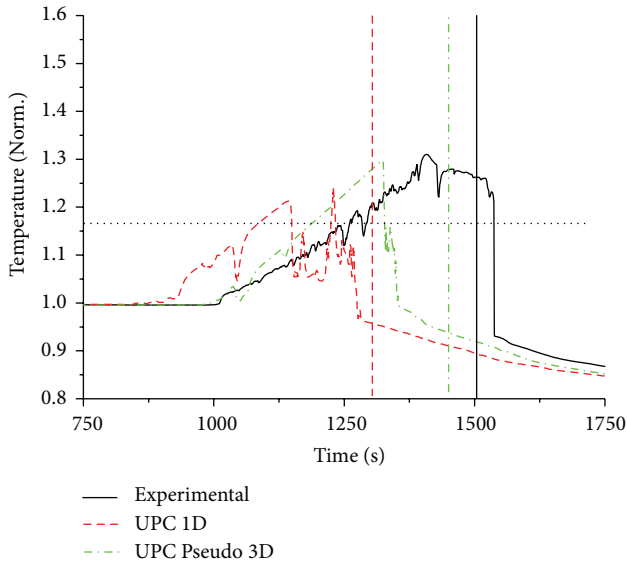
FIGURE 11: Core exit temperature.
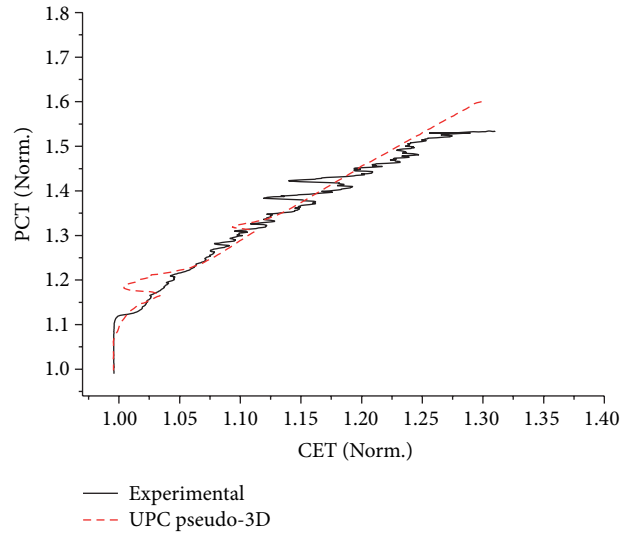
FIGURE 12: PCT versus CET correlation.

3.1 and ROSA Test 3.2 transients [16, 17]. The major features of the vessel nodalization were core and fuel modeled with one channel and one heat structure, respectively; fuel axial core power calculated as an average of the low, medium, and high experimental core power profiles; 9 fuel mesh points; characterization of passive heat structures simulating control rods, core barrel, upper core support plate, instrumentation, and external heat losses.

Results showed a quite good agreement for reproducing initial steady state conditions and main events of three phases of the transient (see Tables 5 and 6). There was a slight overestimation of the break mass losses when stratification appeared in the hot leg, so the break was in two-phase discharging mode (see Figure 13 from 750 s to 1500 s). As a result of this, core uncovery occurred slightly earlier for both phases of the transient (see Table 6), and consequently, the SG depressurization signal related with the CET was activated in advance as well (see Table 6 and Figure 14). In any case, the main parameters were consistently reproduced (see Figures 14, 15, and 16).

Focusing on the relation between the CET and the PCT, results showed a disagreement in the slope of the plots (see Figures 17 and 18). These results suggested that UPC LSTF nodalization should be improved following a similar approach as the one (pseudo-3D modeling) applied in the PKL analysis.

In that sense, a UPC LSTF pseudo-3D nodalization was implemented splitting the core in 13 channels with 18 axial levels (see Figure 19). The low, medium, and high core power axial profiles were simulated, arranging them in each channel as in the experimental radial power distribution. Cartesian crossflows were used for organizing them radially and transversal momentum equations were activated in order to take into account the possible radial ΔP's. Passive HSs were split according to the geometries. Finally, the upper plenum was modified simulating it with two channels, one hot channel, connected to the outlet of the hottest core channel, and another one simulating the rest of the plenum. Transversal momentum equations were activated too in order to consider ΔP's in the vessel that could affect flow path to the hottest channel during the upper plenum HPI injection. On the other hand, HPI mass flow was modified in the conditioning phase in order to match primary mass inventory at the beginning of the low-pressure phase. This correction was justified for the analysis of the following counterpart phases in which the achievement of specified initial conditions is necessary.

TABLE 5: Initial conditions of LSTF Test 3.

	Experimental data (loops w/wo PZR)	UPC-INTE RELAP nodalization (loops w/wo PZR)
Core power (Norm.)	1	1
Hot leg temperature (Norm.)	1	1.001
Cold leg temperature (Norm.)	1	1.003
Mass flow rate (×loop) (Norm.)	1	1.002/0.998
Downcomer-to-hot-leg bypass (Norm.)	1	1
Pressurizer pressure (Norm.)	1	1
Pressurizer liquid level (Norm.)	1	1.014
Secondary-side pressure (Norm.)	1/1	1.004/0.997
Secondary-side liquid level (Norm.)	1	0.995
Main feedwater temperature (Norm.)	1	1
Main feedwater flow rate (Norm.)	1	1.007/1.004
Accumulators pressure (Norm.)	1	1
Accumulators temperature (Norm.)	1	1
LPI pressure (initiation of system) (Norm.)	1	1.24
LPI temperature (Norm.)	1	1
Steam flow rate (Norm.)	1	1.007/1
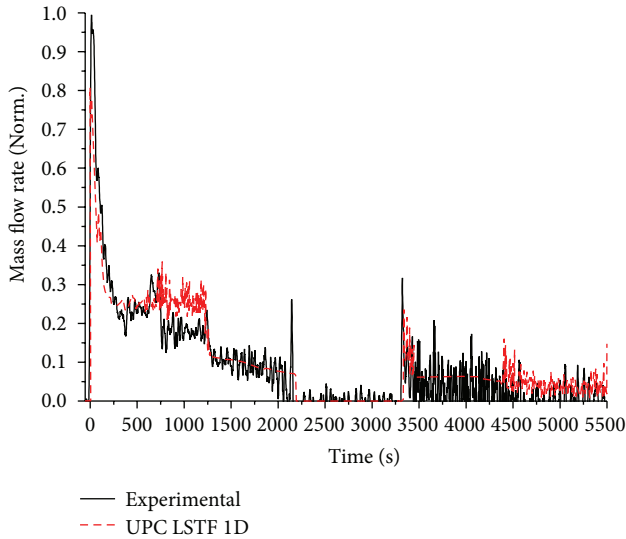
FIGURE 13: Break mass flow.

FIGURE 14: System pressures.

Results of the UPC LSTF pseudo-3D nodalization showed a close agreement in the simulation of the CET versus PCT relationship (see Figures 17 and 18). For both high- and low-pressure transient phases, pseudo-3D nodalization reproduces the same slope and correlation with a margin of 50 and 70 K, respectively, over AM signal established for this particular scenario ($T_{CET} > 623$ K). Regarding core uncovery, the adjustment of initial mass inventory at the beginning of the counterpart phase solves the delay (see low-pressure transient phase of Table 6), obtaining a closer agreement in the simulation of reflux condenser, vapor superheating, and AM phases (see Figure 20).
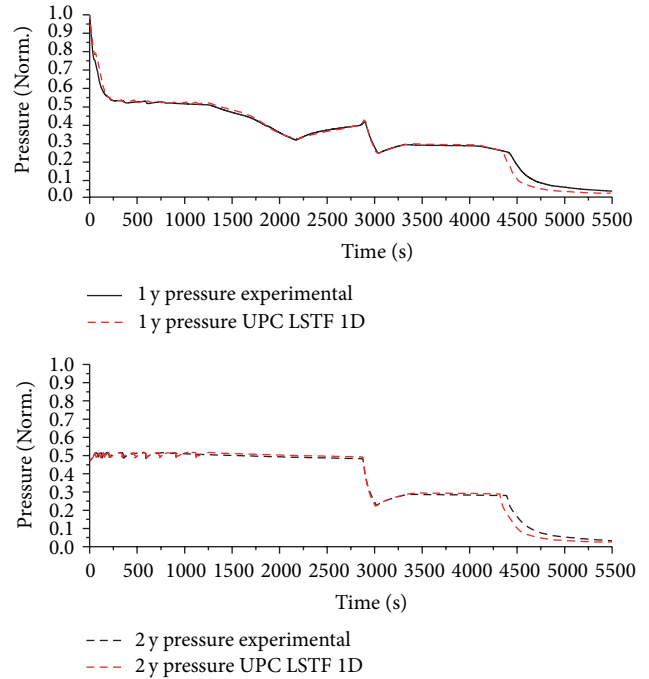
4. "Scaling Effect Analysis" and "Design Effect Analysis" Evaluation

Scaling and design effect analyses are two merged steps of the UPC scaled-up methodology (see Figure 1) in which the analyst can evaluate how the scale and the design modify the results of an ITF simulation. Both steps must only be applied for those phenomena that have been validated for at least two facilities with different scale and design. The effectiveness

TABLE 6: Main events of LSTF Test 3.

Event	Experimental data (s)	UPC LSTF 1D nodalization (s)	UPC LSTF pseudo-3D nodalization (s)
High-pressure transient phase	—	—	—
Break	0	0	0
SCRAM signal	25	33	33
Turbine trip and closure MSIV			
PZR heater off			
Termination main feedwater			
Initiation of coastdown of primary coolant pumps	31	39	39
Termination of continuous opening of SG relief valves, termination of two-phase natural circulation, and break flow from single-phase liquid to two-phase flow	600	1238	1185
Core liquid level starts to decrease (core uncovered)	1545	1460	1475
End high-pressure transient phase (PCT > 750 K)	1840	1852	1778
Conditioning phase	—	—	—
HPI system activated	1850	1862	1788
Break valve closed	2163	2169	2161
HPI system closed	2852	2852	2852
SG depressurization	2880	2892	2880
Termination of SG depressurization	3024	3008	3012
End of Conditioning phase (break valve reopening)	3323	3323	3323
Low-pressure transient phase	—	—	—
Break valve reopening	3323	3323	3323
Primary pressure lower than SG secondary pressure	4108	4085	4105
SG depressurization (CET > 623 K)	4392	4297	4388
Initiation of accumulator system (primary pressure = 2.6 Mpa)	4505	4419	4488
Initiation of LPI system (primary pressure = 1.0 Mpa)	5005	4660	4741
End of the transient	5500	5500	5500

of these techniques has been checked taking advantage of the posttest calculations described above. In that sense, PKL-LSTF counterpart test becomes useful in that it relates two facilities to different scale and design (see Table 1).

Once the posttest analyses are described, the experimental differences reported in Section 2.3.3 must be checked in order to guarantee the validation of the related phenomena in the simulation. The following can be concluded.

(i) CET versus PCT correlation discrepancies: UPC LSTF and PKL nodalizations were qualified for simulating CET versus PCT correlation in that they reproduce the phenomenon with close results (see Figures 12, 17, and 18).

(ii) Core dryout delay: once initial mass inventory was readjusted in the LSTF pseudo-3D nodalization for the low-pressure transient phase, the results of both simulations showed a quite good agreement in the reproduction of the core uncovery (see Tables 4 and 6), reproducing qualitatively well the timing of the three phases of the transient in each case. The same criteria were applied in both nodalizations for the modelling of the core (which affects vapor generation)

and the break (which affects primary mass inventory); therefore, both simulations were qualified showing a qualitative consistency with respect to experimental data in at least two different facilities.

(iii) SG depressurization effectiveness: results of the PKL simulation showed the inefficacy of UPC PKL nodalization for reproducing the effect of the SG depressurization in the CET (see Figure 11). For this case, PKL nodalization is not qualified and no further analysis can be done.

4.1. Scaling Effect Analysis. The aim of the scaling effect analysis step is to generate an idealized ITF scaled-up nodalization in which the effects of the scaling are minimized. ITF posttest calculation must be scaled to the size of the analyzed facility/NPP nodalization following the scaling criteria applied in the design of the experimental facility. The reported distortions of the scaling criteria must be studied in order to evaluate how they modify the results and in order to generate an idealized input deck without their effects. Only in the case where the scaling effects have been removed, the design effects can be analyzed.
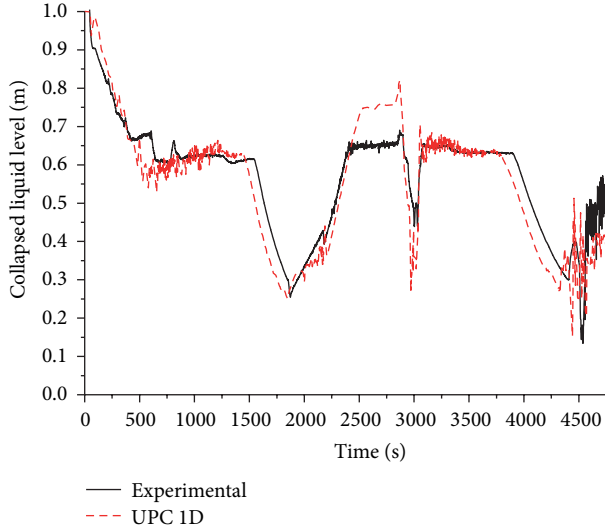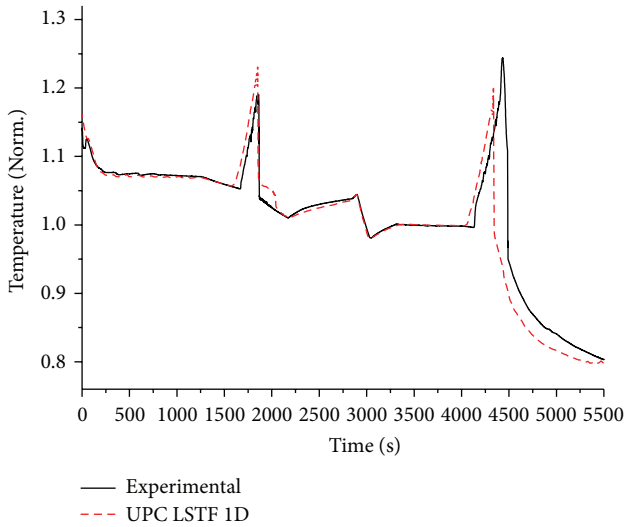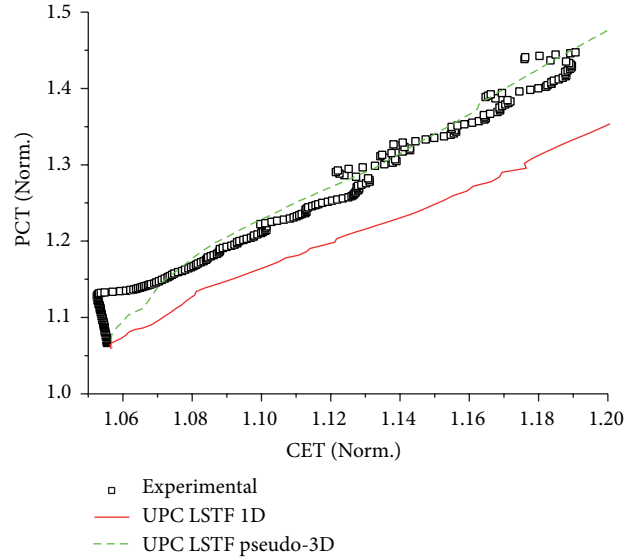
Figure 15: Core level.

Figure 16: Core exit temperature.

Figure 17: PCT versus CET curve during high-pressure transient phase.
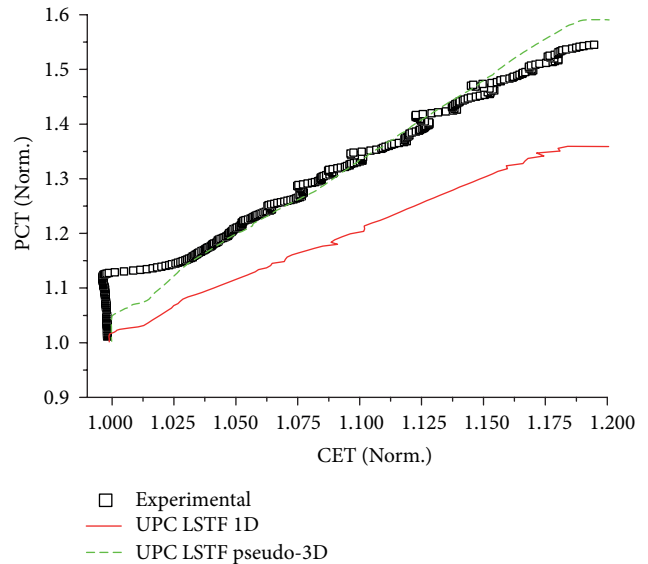
Figure 18: PCT versus CET during low-pressure transient phase.

In the case of the PKL and the LSTF experimental facilities, the power-to-volume scaling method was followed for their design. For this criterion, scaling distortions are mainly related to changes in hydraulic diameter, which affects the external heat losses, energy storage in passive structures, friction effects, and flow regime transitions (for more detailed information see the related paper [8]). For analyzing scaling effects of the counterpart test, PVST software (general description in paper [8]) has been applied to the validated UPC PKL pseudo-3D nodalization.

As a first step, a nodalization (named Sc-up nodalization A) has been generated using the PKL-LSTF K_v factor suggested by the PKL and LSTF operator agents. This nodalization follows the power-to-volume (PtoV) scaling criterion, so that a PKL nodalization has been obtained with the same size in power and in volume as of those of LSTF. The comparison

between Sc-up nodalization A and the UPC PKL pseudo-3D nodalization shows discrepancies in the system pressures during reflux condenser and vapor superheating phases (see Figure 21) despite having similar mass discharged through the break (see Figure 22: the slight discrepancy is because primary pressures are not equal). The secondary pressure is higher for Sc-up nodalization A, pushing up the coupled primary pressure during reflux condenser phase.

In order to analyze this distortion, a new nodalization, Sc-up nodalization B, is generated. This is a PKL PtoV scaled-up nodalization (as Sc-up nodalization A) in which the heat impact of external heat structures has been preserved. The comparison between the two posttest calculations of Sc-up
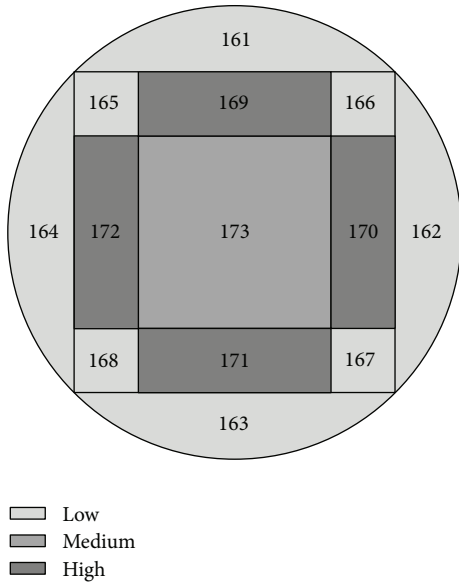
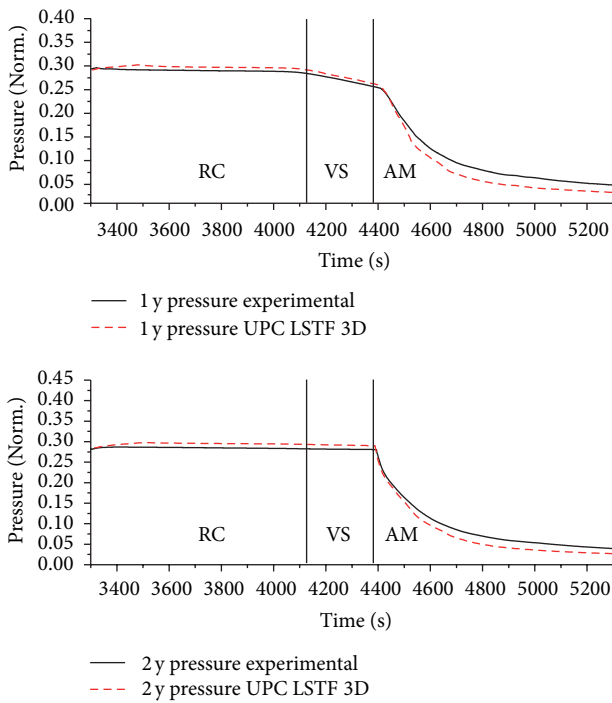FIGURE 19: UPC LSTF pseudo-3D nodalization core channels.

FIGURE 20: System pressures.

FIGURE 21: System pressures.

nodalization A and Sc-up nodalization B confirms that a distortion should be expected in the system pressures as a result of the reduction in the external heat losses (see Figure 21). Because the external heat losses are reduced when PtoV scale is increased, part of this energy is stored in the isolated secondary system, increasing pressures during reflux condenser phase.
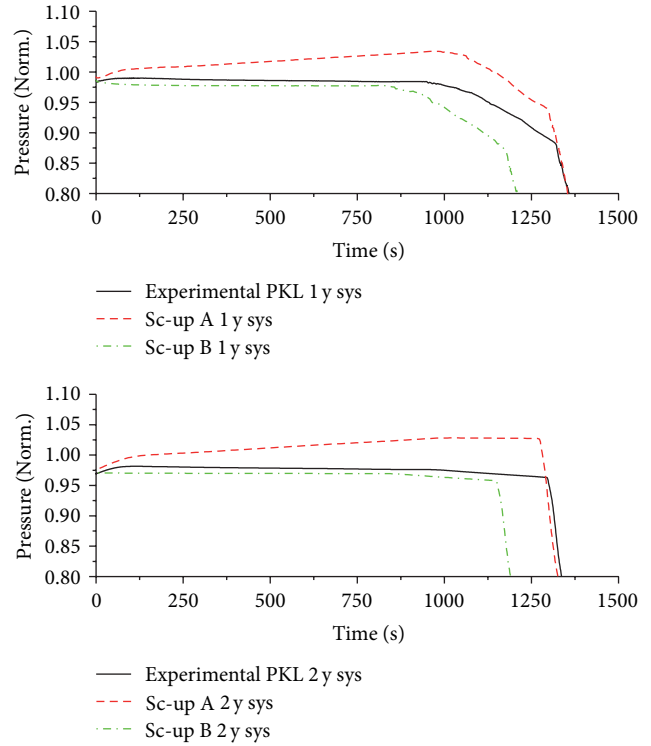
Once the external heat losses distortion is corrected, a discrepancy appears in the timing of the SG depressurization signal (see Figure 21). Taking into account that the aim of the scaling effect analysis is to generate an idealized PKL scaled-up nodalization in which scaling effects are minimized, another scaled-up nodalization must be generated following the previous nodalizations. Therefore, a third nodalization Sc-up nodalization C is produced based on Sc-up nodalization B but with the additional preservation of the $L/\sqrt{D}$ quotient in the hot legs. Keeping this ratio in the horizontal legs, the Froude number and the flow regime transitions should be preserved. The comparison between the PKL posttest calculation and the results obtained by Sc-up nodalizations B and C shows that the hot leg liquid levels in the broken loop are preserved for Sc-up nodalization C during the conditioning phase of the PKL transient (see in Figure 23 from −4000 s to −3500 s and from −2750 s to −2500 s intervals), thus providing similar break mass flow rates as in the posttest calculation (see Figure 24). This allows keeping the same primary mass inventory ratio at the beginning of the transient, obtaining similar liquid levels in the hot leg of the broken loop (see Figure 25) and similar break mass flow rates (see Figure 26). This good performance of the mass discharging removes the delay in the core uncovery obtaining a close agreement in the timing of the SG depressurization (see Figure 27).

After removing the Froude number distortion, the main parameters of the transient are compared between UPC PKL
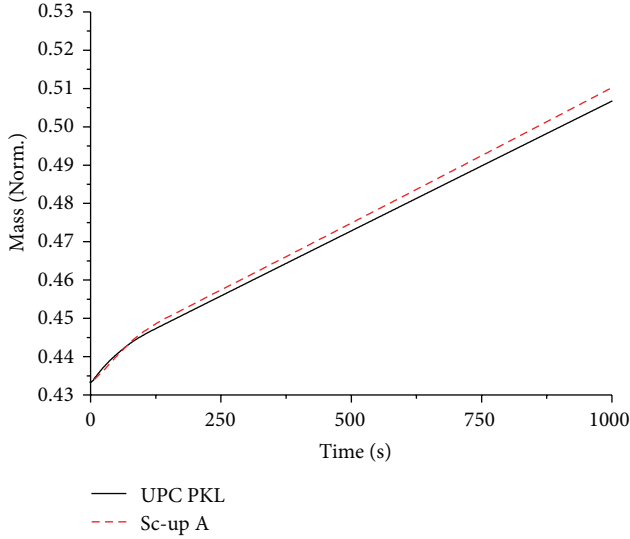
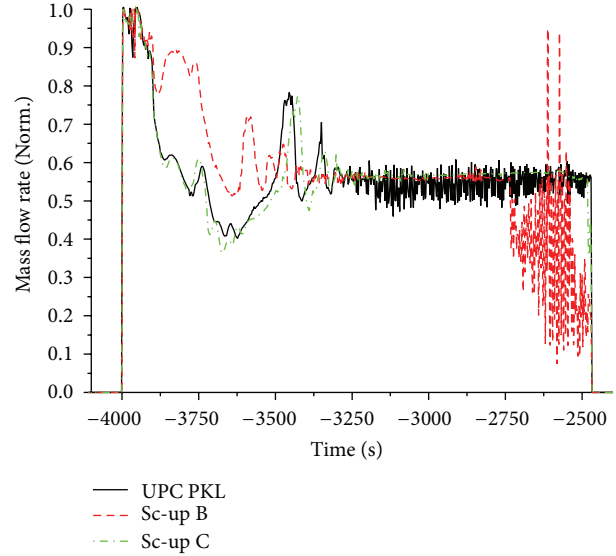FIGURE 22: Mass discharged through the break.
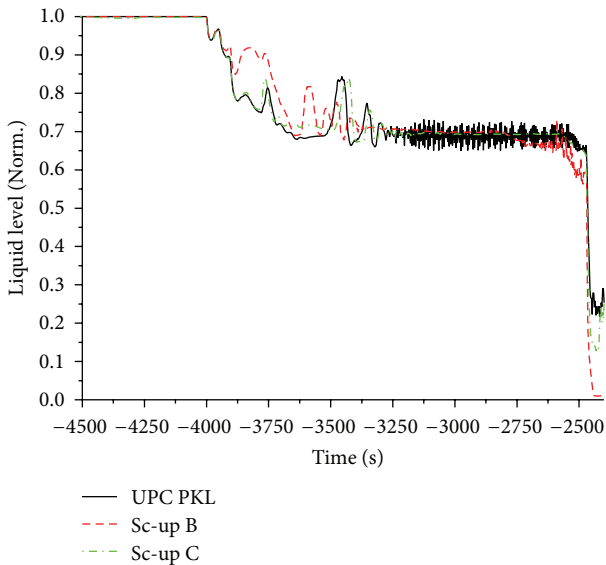

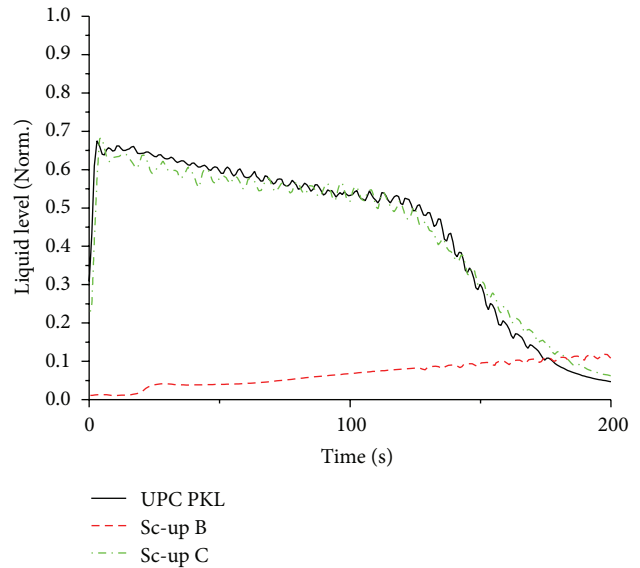FIGURE 24: Break mass flow rate.

FIGURE 23: HL liquid level.

FIGURE 25: HL liquid level.

pseudo-3D nodalization calculation and the Sc-up nodalization C calculation in order to assure that an idealized scaled-up nodalization has been obtained. Results of the system pressures (Figure 27), CET temperatures (Figure 28), and PCT temperatures (Figure 29) display a close agreement between the posttest and Sc-up nodalization C. Since the discrepancies to be analyzed between PKL and LSTF simulations are the core uncovery delay and the CET versus PCT correlation, no further scaling effect analysis will be necessary. Friction effects or hydraulic diameters in components where mixing or interface drag occurs (i.e., SG and vessel downcomers) could be studied until a perfect idealized scaled-up nodalization is obtained, but as for this transient, they will not add any relevant scaling effect in the reported LSTF-PKL discrepancies, it would suppose an unnecessary extra work

for the analyst. It is in that point where the expert judgment is essential.

4.2. Design Effect Analysis. Once an idealized PKL scaled-up nodalization has been generated, discrepancies between both counterpart simulations can be analyzed. For this purpose hybrid nodalizations will be compared with qualified LSTF posttest simulation and the idealized PKL scaled-up nodalization. Hybrid nodalizations will include LSTF components in the PKL nodalization in order to check how they modify the results.

4.2.1. Core Dryout Delay. The comparison between UPC LSTF pseudo-3D nodalization and *PKL* idealized scaled-up
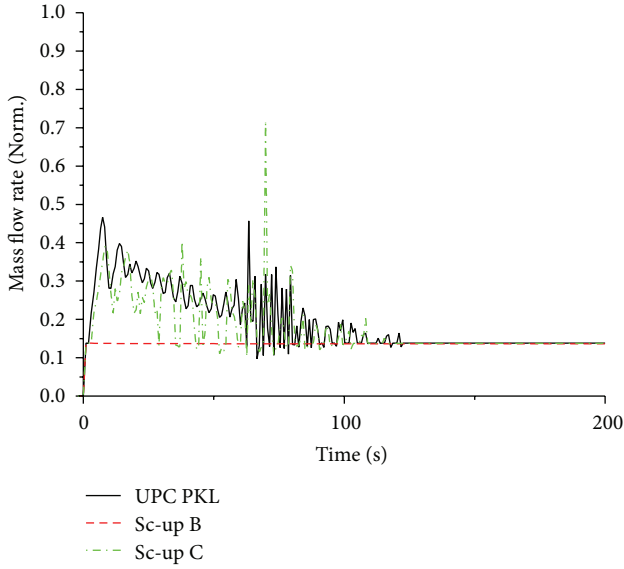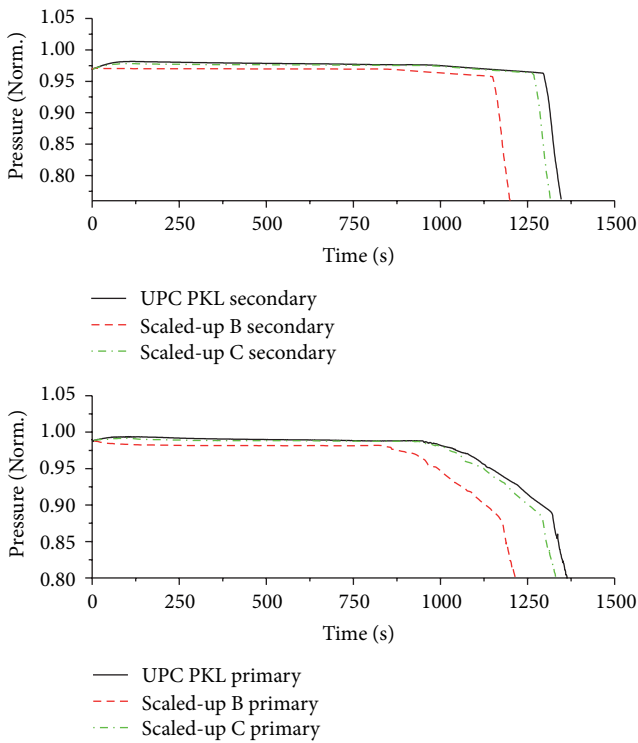
FIGURE 26: Break mass flow rate.

FIGURE 27: System pressures.

FIGURE 28: Core Exit temperature.

FIGURE 29: Peak cladding temperature.

nodalization (Sc-up nodalization C of the previous step) shows a disagreement in the core dryout timing despite having a similar amount of water in the primary system (see Figures 30 and 31). For analyzing this discrepancy a *PKL* hybrid base nodalization has been generated in order to adapt those scaling effects reported in the previous steps to the intrinsic design characteristics of the LSTF facility. I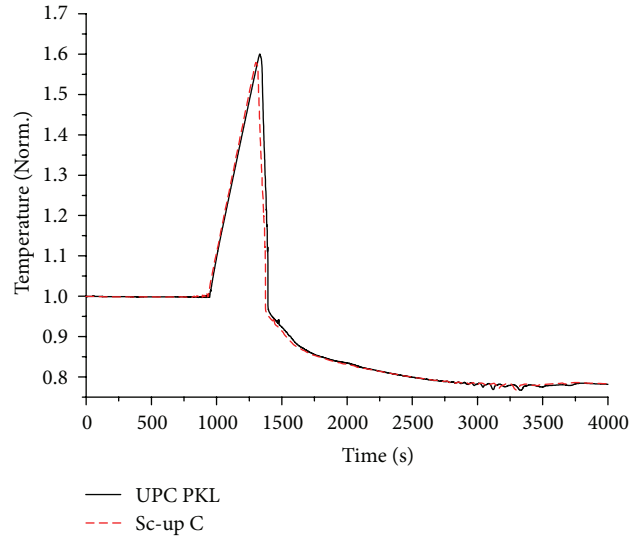n other words, the idealized PKL scaled-up nodalization is modified by adding the LSTF external heat losses, merging 4 loops into 2 loops, and adjusting the hot leg geometries in order to preserve the LSTF $L/\sqrt{D}$ factor and finally by removing the compensating heaters during the transient as in the LSTF conditions. The comparison between the 3 nodalizations shows that the external heat losses and the different hot leg geometries do not justify the delay between both nodalizations (see Figure 32).

For analyzing the discrepancy, components with different configuration that could affect the mass inventory and distribution have been studied. Those are as follows.

(i) Pressurizer and surge line: PKL surge line is not connected at the bottom of the pressurizer as in LSTF facility. During the blowdown, some water can remain stagnant below the connection anticipating the core dryout.
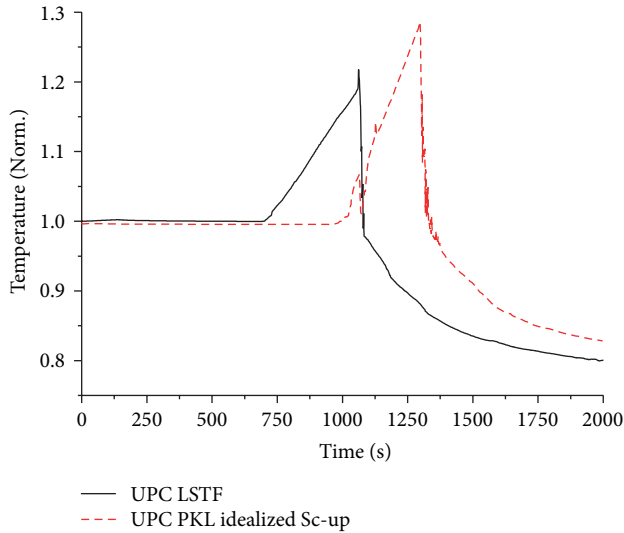
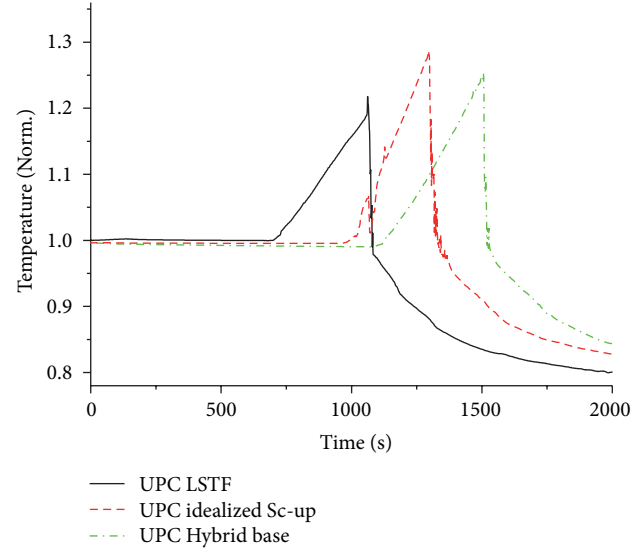FIGURE 30: Core exit temperature.

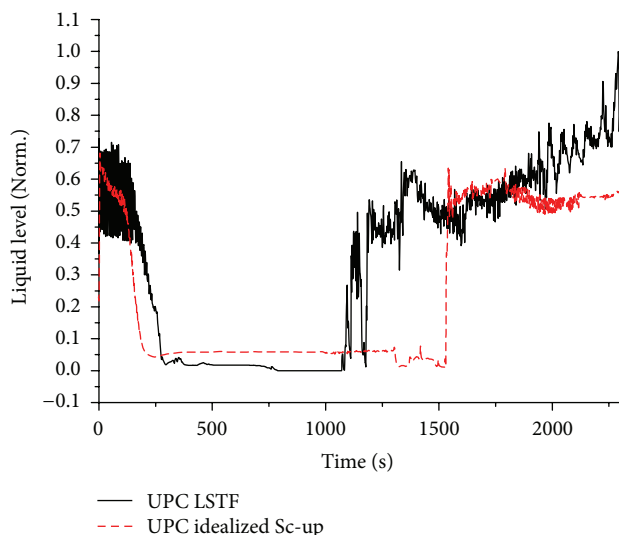FIGURE 32: Core exit temperature.

FIGURE 31: HL liquid level.

Four hybrid nodalizations are performed in series adding one to one these LSTF components to the PKL hybrid base nodalization. The aim is to analyze, one by one and globally, how they modify the timing of the core dryout. The nodalizations are

(i) PKL Hybrid A nodalization: PKL Hybrid base nodalization + LSTF PZR;

(ii) PKL Hybrid B nodalization: PKL Hybrid A nodalization + LSTF U-tubes surface;

(iii) PKL Hybrid C nodalization: PKL Hybrid B nodalization + LSTF HL-to-DC bypass;

(iv) PKL Hybrid D nodalization: PKL Hybrid C nodalization + LSTF vessel passive HS.

The results of hot leg liquid levels and CET (Figures 33 and 34) show that there are no changes in the core dryout timing despite adding LSTF components to the PKL hybrid base nodalization. It demonstrates that these design differences do not have an effect on the reported discrepancy.

Finally, the vessel characteristics have been compared between both nodalizations, showing relevant differences in the configuration of the downcomer, the simulation of the core bypass flow path, and, specially, the amount of water between the bottom of the hot leg and the top of the core (these features are described in Table 7). Hence, a Hybrid E nodalization is generated adding to the "PKL Hybrid D nodalization" hydrodynamic components, HSs, and material properties of the LSTF vessel nodalization. The PKL fuel rods HSs are not modified. The results obtained with this new nodalization show that, for an identical amount of water in the hot legs at the beginning of the transient (for having the same PKL experimental initial conditions despite the changes in the nodalizations), the core dryout occurs at the same time as that of the LSTF posttest calculation just changing the water distribution of the PKL vessel with that of the LSTF vessel (see Figures 35 and 36). It demonstrates that delay

(ii) U-tube's surface: LSTF and PKL have different ratio between liquid volume and heat exchanging surface (LSTF U-tube surface = 1.01 PKL U-tube surface) that could affect the reflux and condensation and the total amount of water in the primary side.

(iii) LSTF DC-to-HL bypass: LSTF has an external bypass not simulated in PKL which could imply different water distribution between hot legs and cold legs. It could modify break mass losses advancing or delaying core dryout.

(iv) Core passive heat structures: LSTF and PKL have different volume of core passive structures, which could affect the vapor generation and core liquid levels.
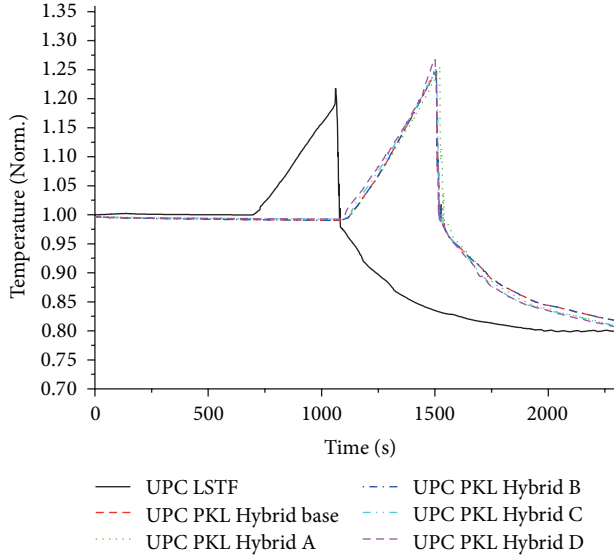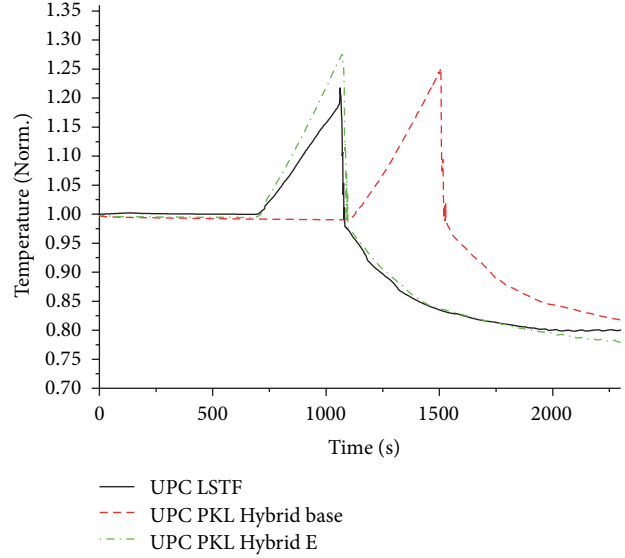
FIGURE 33: Core exit temperature.
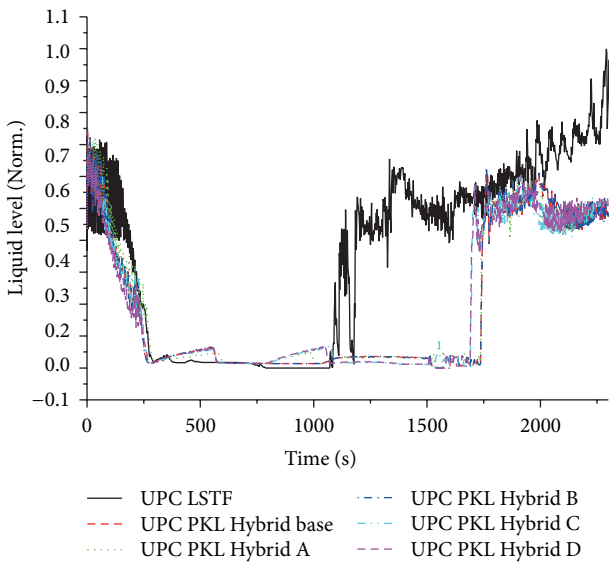

FIGURE 35: Core exit temperature.

TABLE 8: Core design differences.

	LSTF	PKL
Axial profile	Cosine	Flat
Radial profile	3	1
Fuel diameter (mm)	4.75	5.375
Fuel height (m)	3.66	3.9
Fuel surface (m^2)	55.054	52.73 ($\cdot Kv$)
Number of rods	1008	801 ($\cdot Kv$)

Two new PKL hybrid nodalizations are set up from the previous PKL Hybrid E nodalization in order to justify the discrepancy. Main characteristics are

(i) previous PKL Hybrid E nodalization:

    (a) LSTF vessel HSs and hydrodynamic components,
    (b) PKL fuel rods HSs,
    (c) PKL fuel rods materials,
    (d) PKL fuel rods profile (uniform);

(ii) PKL Hybrid F nodalization:

    (a) PKL Hybrid E nodalization

      (1) LSTF fuel rods HS's
      (2) LSTF fuel rods materials;

(iii) PKL Hybrid G core nodalization:

    (a) PKL Hybrid F nodalization

      (1) LSTF fuel rods profile (cosine).

The comparison of the three hybrid nodalizations with both LSTF and PKL posttest calculations (Figure 37) demonstrate that the discrepancies in the slope of CET versus PCT

FIGURE 34: HL liquid level.

TABLE 7: LSTF and PKL vessel differences.

	LSTF	PKL
Downcomer	Annulus	2 pipes
Core bypass	No	Yes
Mass inventory below hot leg	$\cong 0.75 \cdot MPKL$	MPKL

between core dryout of both simulations is due to the different design of the vessel (KWU for PKL and Westinghouse for LSTF) and not for any scaling effect.

4.2.2. CET versus PCT Correlation. Major LSTF-PKL core design differences are shown in Table 8.
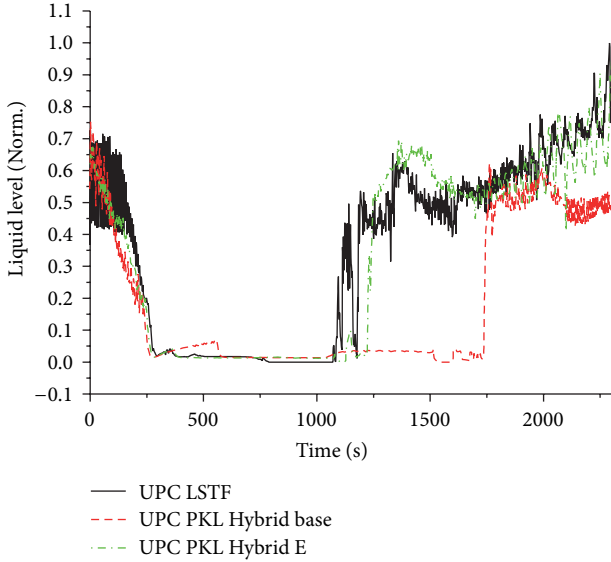
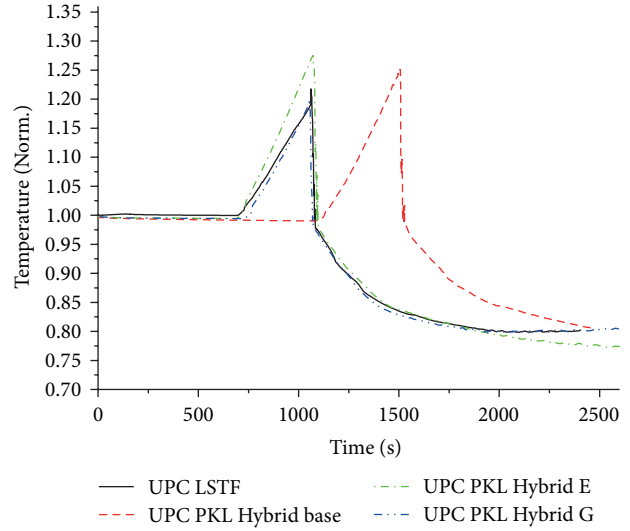Figure 36: HL liquid level.
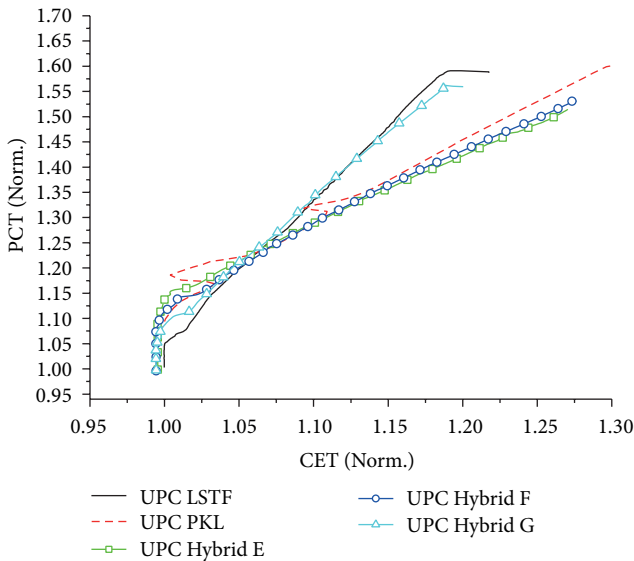

Figure 38: Core exit temperature.

Figure 37: PCT versus CET curve.

curves are mainly due to the different power distributions of PKL (uniform) and LSTF (cosine). As modifications between hybrid models have been implemented in a serial process, just when PKL core power profile is modified (PKL hybrid nodalization G), the slope of the curve becomes similar to the LSTF posttest CET versus PCT slope. On the other hand, previous changes (models E and F) do not show significant modifications in the CET versus PCT correlation.

Finally, CET of the last nodalization (PKL Hybrid G nodalization) is compared (Figure 38) with the nodalization that justifies the delay in the core dryout (PKL Hybrid E nodalization). Results show that new modifications do not add distortion, justifying the consistency of the procedure.

5. Conclusions

The UPC scaling-up methodology has been applied for analyzing discrepancies that appear between the simulations of two counterpart tests. The conclusions related to the quality assurance of system codes modeling can be divided into two blocks, one related to the relevance of the ITF simulations and posttest analyses and the other one related to the guidelines of the proposed methodology for relating counterpart NPP scaled calculations (also known as K_v-scaled analysis; see [18]) and ITF posttest simulations.

In regard to the simulation of ITF tests, the present paper has demonstrated that posttest analyses and counterpart simulations are unavoidable in order to qualify the NPPs modeling criteria which the analyst applies for characterizing the NPP nodalization. Experimental data give the opportunity to improve ITF nodalizations for selected phenomena and scenarios, and, on the other hand, counterpart tests permit studying their consistency over different scales and designs. Only those phenomena that have been well reproduced using the same modeling criteria at different ITFs can be used for establishing modeling conclusions for qualifying and improving NPP nodalizations. About this point, the results of the present paper show how the LSTF-PKL counterpart tests have allowed the analyst to define which phenomena could be well reproduced by their nodalizations (CET versus PCT correlation) and which not (quenching during SG fast depressurization), in this way establishing the basis for a future extrapolation to an NPP scaled calculation.

In addition, the UPC scaling-up methodology has been checked over two counterpart simulations that were previously qualified with experimental data. The application of the scaling effect and design effect analysis described in [8] has demonstrated that selected phenomena can be perfectly scaled up between counterpart simulations by carefully considering the differences in scale and design. In relation

to this, scaled-up and hybrid nodalizations can be used in order to scale results and predict the source of the possible discrepancies.

Future work will be devoted to show an application of the UPC scaled-up methodology for qualifying a commercial NPP nodalization over selected phenomena of LSTF-PKL counterpart tests.

Nomenclature

1D:	One-dimensional
3D:	Three-dimensional
ACC:	Accumulator
AM:	Accident management
CET:	Core exit temperature
CL:	Cold leg
D:	Pipe diameter
DC:	Downcomer
ECCS:	Emergency core coolant systems
HL:	Hot leg
HPI:	High-pressure injection
HS:	Heat structure
IAEA:	International Atomic Energy Agency
ITF:	Integral test facility
K_v:	Scaling factor
KWU:	Kraftwerk Union
L:	Length
LOCA:	Loss-of-coolant accident
LPSI:	Low-pressure safety injection
LPI:	Low-pressure injection
LSTF:	Large-Scale Test Facility
NEA:	Nuclear energy agency
NPP:	Nuclear power plant
OECD:	Organization for Economic Cooperation and Development
PCT:	Peak cladding temperature
PKL:	Primärkreislauf
PtoV:	Power-to-volume
PVST:	Power-to-volume scaling tool
PZR:	Pressurizer
RC:	Reflux condenser
ROSA:	Rig of safety assessment
SBLOCA:	Small break loss-of-coolant accident
SG:	Steam generator
t:	Time
UMAE:	Uncertainty method based on accuracy extrapolation
UPC:	Universitat Politècnica de Catalunya
USNRC:	United States Nuclear Regulatory Commission
VS:	Vapour superheating.

Conflict of Interests

The authors declare that there is no conflict of interests regarding the publication of this paper.
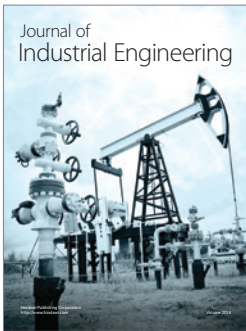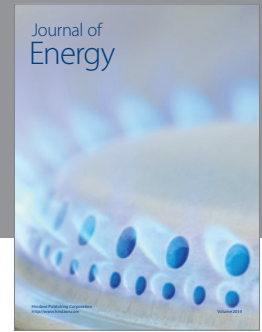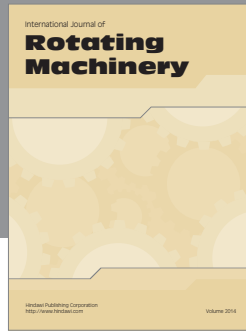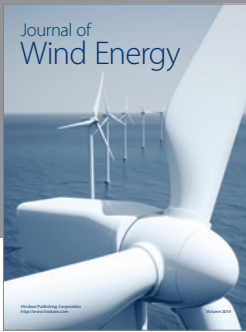
Acknowledgments

References

[1] "Accident analysis for nuclear power plants," Safety Reports Series 23, IAEA, Vienna, Austria, 2002.

[2] "Development and review of plant specific emergency operating procedures," Safety Reports Series 48, IAEA, Vienna, Austria, 2006.

[3] F. Reventos, "Thermal-hydraulic analysis tasks for ANAV NPPs in support of plant operation and control," *Science and Technology of Nuclear Installations*, vol. 2008, Article ID 153858, 13 pages, 2008.

[4] F. Reventós, C. Llopis, L. Batet, C. Pretel, and I. Sol, "Analysis of an actual reactor trip operating event due to a high variation of neutron flux occurring in the Vandells-II nuclear power plant," *Nuclear Engineering and Design*, vol. 240, no. 10, pp. 2999–3008, 2010.

[5] C. Llopis, F. Reventós, L. Batet, C. Pretel, and I. Sol, "Analysis of low load transients for the Vandellòs-II NPP. Application to operation and control support," *Nuclear Engineering and Design*, vol. 237, no. 18, pp. 2014–2023, 2007.

[6] F. Reventós, L. Batet, C. Llopis, C. Pretel, M. Salvat, and I. Sol, "Advanced qualification process of ANAV NPP integral dynamic models for supporting plant operation and control," *Nuclear Engineering and Design*, vol. 237, no. 1, pp. 54–63, 2007.

[7] A. Cuadra, J. Gago, and F. Reventos, "Analysis of a main steam line break in ascó nuclear power plant," *Nuclear Technology*, vol. 146, no. 1, pp. 41–48, 2004.

[8] V. Martinez-Quiroga and F. Reventos, "The use of system codes in scaling studies: relevant techniques for qualifying NPP nodalizations for particular scenarios," *Science and Technology of Nuclear Installations*, vol. 2014, Article ID 138745, 13 pages, 2014.

[9] H. Kremin, H. limprecht, R. Güneysu, and K. Umminger, "Description of the PKL III test facility," Framatome ANP Report, 2001.

[10] The ROSA-V Group, "ROSA-V Large Scale Test Facility (LSTF) system description for the third and fourth simulated fuel assemblies," Technical Report JAERI-Tech 2003-037, Japan Atomic Energy Agency, 2003.

[11] J. Freixa, F. Reventós, C. Pretel, L. Batet, and I. Sol, "SBLOCA with boron dilution in pressurized water reactors. Impact on operation and safety," *Nuclear Engineering and Design*, vol. 239, no. 4, pp. 749–760, 2009.

[12] J. Freixa, *SBLOCA with boron dilution in pressurized water reactors. Impact to the operation and safety [Ph.D. thesis]*, Universitat Politècnica de Catalunya, DFEN, 2007.

[13] J. Freixa, F. Reventós, C. Pretel, and L. Batet, "Boron transport model with physical diffusion for RELAP5," *Nuclear Technology*, vol. 160, no. 2, pp. 205–215, 2007.

[14] F. Reventós, J. Freixa, L. Batet et al., "An analytical comparative exercise on the OECD-SETH PKL E2.2 experiment," *Nuclear Engineering and Design*, vol. 238, no. 4, pp. 1146–1154, 2008.

[15] "RELAP5/MOD3 Code manual. Volume II: Appendix A Input Requirements," NUREG/CR-5535/Rev.1, ISL, Idaho, USA, January 2003.

[16] V. Martínez, F. Reventós, and C. Pretel, "Post-Test Calculation of the ROSA/LSTF Test 3-1 using RELAP5/mod3.3," NUREG/IA-409, 2012.

[17] V. Martínez, F. Reventós, and C. Pretel, "Post-Test Calculation of the ROSA/LSTF Test 3-2 using RELAP5/mod3.3," NUREG/IA-410, 2012.

[18] F. D'Auria and G. M. Galassi, "Scaling in nuclear reactor system thermal-hydraulics," *Nuclear Engineering and Design*, vol. 240, no. 10, pp. 3267–3293, 2010.